OUTAGE PERFORMANCE OF RIS-AIDED FSO-BASED GROUND-AIR INTEGRATED VEHICULAR NETWORKS

Nguyen Van Thang and Pham Thi Thuy Hien
Posts and Telecommunications Institute of Technology

***Abstract*—**Significant obstacles to the practical design of free-space optical communications (FSOs) include atmospheric turbulence and pointing problems. Reconfigurable intelligent surface (RIS) is an emerging technology that uses inexpensive inactive reflecting materials to intelligently gently change the beam in the appropriate direction, enabling reflective radio transmission conditions for next-generation 5G/6G wireless frameworks. In this study, we suggested an FSO system with RIS assistance to mitigate the effects of signal blockage in the communication system, atmospheric turbulence, and UAV's misalignment-induced fading. In a free-space environment with obstacles, the probability density function and cumulative distribution functions of an FSO system made up of RIS are derived. We obtained closed-form formulas for the outage probability of the proposed system. The performance analysis of the considered system under different weather conditions, pointing errors, and RIS vibration is done in terms of the outage probability. The findings are presented in relation to the transmitted power, the transmission distance, and the outage performance. Because the considered system will offer dependable connectivity in urban settings with dense populations and tall structures, it will be advantageous for the ground-air integrated vehicular network applications.

***Keywords*—** Reconfigurable intelligent surface (RIS); Free-space optical (FSO); Vehicular network**.**

I. INTRODUCTION

Nowadays, more than half of the world's population resides in cities, with an increasing number of them being densely inhabited. Urbanization is one of the biggest shifts that has affected human civilization and its living environment, along with industrialization and economic development. The hubs of human social and economic activity are cities. As a result of the development of science and technology, city dwellers' ways of living have evolved together with human civilization [1, 2]. Ensuring individuals have long-term access to buildings, infrastructure, and vital services is critical. The urban area model is being considered by many well-known cities throughout the world in an effort to enhance living conditions for citizens and maximize the use of resources and infrastructure. Intelligent services that support better performance and operations in transportation, healthcare, education, and other fields can be provided thanks to a range of modern technologies. These services assist smart cities in reducing operating costs and maximizing the use of available resources [3]. Information and communication technology integration is the foundation of the urban area concept as a whole. Communication technologies used in smart cities to provide wired and wireless connectivity include millimeter wave, terahertz, radio frequency, and free-space optical communication (FSOC). Of them, FSOC is most frequently used because of its cheap cost, high data rate, bandwidth, and license-free nature.

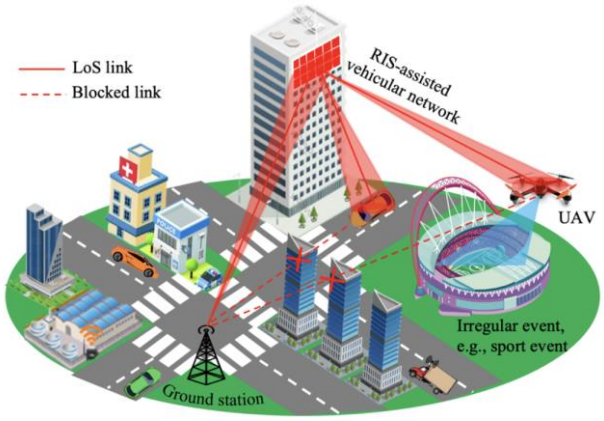

Figure 1. RIS-assisted FSO system for vehicular network.

Since the traditional FSOC architecture depends entirely on a line-of-sight (LOS) component, alignment between the transmitter and receiver is never easy, especially in urban areas. System's performance decrease results from misalignment and pointing errors as a result of this requirement [4]. The deployment of a building-to-building FSOC communication system or a terrestrial FSOC link is inherently difficult due to the constant presence of obstacles and unavailability of clear line-of-sight paths. Due to atmospheric turbulence, occlusion from blockages, and the pointing error phenomenon that a beam

Tác giả liên hệ: Nguyen Van Thang,
Email: thangnv@ptit.edu.vn
Đến tòa soạn: 10/2023, chỉnh sửa: 11/2023, chấp nhận đăng: 12/2023.

experiences in the medium, the performance of an FSOC system deteriorates with distance. To learn more about how these disruptions affect the FSOC signal's behavior, one can take a closer look at the behavior in real time. For FSOC systems, which are mounted on the roof of a multistory building, the pointing inaccuracy phenomena is typically observed. Pointing mistakes are caused by weak earthquakes, strong winds blowing toward the transmitter/receiver, and other prevailing variables [5]. As a result of mismatched fading and diffraction, the source will be momentarily obstructed and unable to connect with the destination, leading to random and bursting errors.

Reconfigurable intelligent surface (RIS) is a novel project that uses micro-controller units and meta-surfaces to reflect electromagnetic waves and optical signals in the appropriate direction [6]. This technology's main benefit is that it can improve and regulate the emitted beam's feasible properties, including its frequency, phase, and intensity [7]. In order to provide a real-time re-configurable propagation environment, RIS, which is made up of passive and inexpensive parts, may efficiently alter the phase, frequency, amplitude, and even polarization of the impinging signal [8]. The module can function in special circumstances by manipulating the optical beam with the aid of a RIS structure, depending on the communication design framework. Specifically, depending on the angle of arrival and angle of departure, the RIS module can be utilized to reflect and beamform to a particular receiver [9]. A review of an underwater wireless optical communication link that makes use of both RIS and conventional direct links is provided in [10]. In [11], the performance metrics of a triple-hop RIS-assisted RF-FSO convergent with underwater wireless optical communication system were given and examined. The authors of [12] used a coherent array optical transmitter for a 20-deg angular range signal reflection to show an experimental non-line-of-sight FSO link with an optical-phased-array RIS. The primary benefit of RIS-based FSOC is an improved signal quality and extended link range [13]. The literature has included selection beamforming techniques to facilitate the formation of a communication link via a non-line-of-sight communication path [14]. In order to improve coverage and reliability, the authors of a recent paper [15] suggested a multiuser communication strategy that uses the RIS to improve a sizable group of multiple input multiple output antennas and extrapolate the beam in the designated direction. To determine the system data rate, the authors in [16] examined the performance using constrained phase shifts. The system total rate is entirely reliant on the RIS's size, as seen in [16]. The performance of RIS in dual-hop decode and forward relay empowered asymmetric RF/FSO systems was examined by the authors in [17]. Assuming intensity modulation, the authors of [18] looked at the unified first- and second-order performance evaluation of an FSO RIS-assisted communications connection over F-S F turbulence-induced fading channels.-fading channels in different situations of TI fading severity.

In this study, we present a RIS-based FSO system for ground-air integrated vehicular networks. The effectiveness of the suggested method is examined when propagation loss, pointing error effects, and atmospheric turbulence are present. To model the behavior of atmospheric turbulent channels, we employed the gamma-gamma distribution function. In order to handle moderate to high atmospheric turbulence regimes, it is frequently used in FSOC [19–21]. The following are the contributions made by this work.

- In the presence of RIS-vibration, UAV hovering, atmospheric turbulence, the cumulative distribution function (PDF) and probability density function

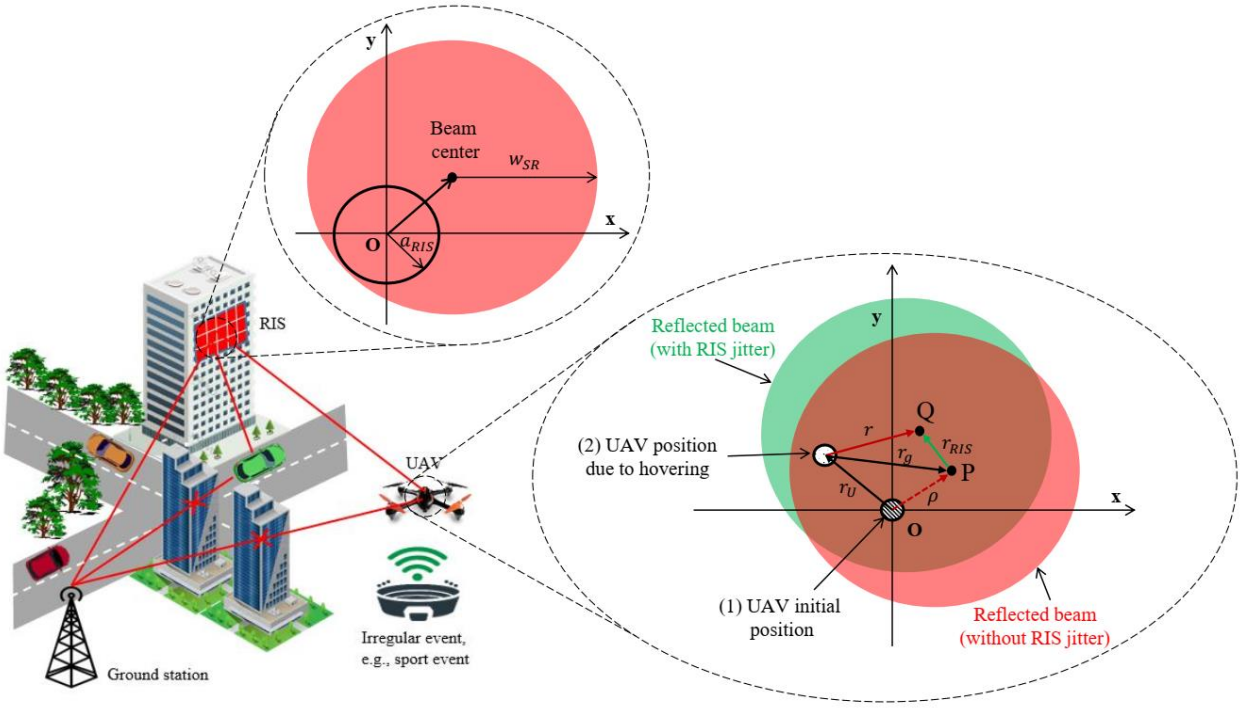

Figure 2. RIS vibration induced fading modeling.

(PDF) of the combined channel model are derived.
- Performance analysis is done on the outage probability of RIS-assisted FSO-based ground-air integrated vehicular networks.
- We looked at the outage probability performance of the RIS-assisted FSO link and finding the optimum value for the system parameter to reach the target.

The remainder of the document is structured as follows: The concept of the system and channel model is presented in Section 2; system performance is explained in Section 3; and findings are discussed in Section 4. In Section 5, we offer some futuristic thoughts to wrap up the paper.

II. SYSTEM AND CHANNEL MODEL

A. System model

We consider an RIS-assisted FSO-based ground-air integrated vehicular network, in which the system has certain robustness to obstacles or long channel length with the help of RIS as shown in Fig. 1. The source node (S) communicates with a destination node (D) via RIS with reflecting elements, and it is assumed the direct links between transmitter and receiver are blocked due to obstructions. RIS is positioned in building wall as a relay node and then multiple controllable optical channels are constructed without extra demand for equipment.

Each RIS element receives incident waves and forwards the signal to the desired receiver by adjusting phase and amplitude shift controlled by a programmed controller. Assuming full reflecting and full phase compensation, the signal received at the destination can be written as,

$$y = hgx + n, \tag{1}$$

where x is the transmitted signal with power P_t. h and g denote the channel fading coefficients between transmitter to i-th reflecting surface and i-th reflecting surface to receiver, respectively. $n \sim N(0, N_0)$ is the additive white Gaussian noise (AWGN) with zero mean and variance N_0. The random variables $h = h_a h_t h_p$ and $g = g_a g_t g_p$ are assumed to be independent and non identically distributed, which include the effect of atmospheric attenuation, atmospheric turbulence, and pointing error.

B. Propagation Loss

The composed of gas molecules and aerosol particles in the atmosphere severely affect the FSO link by absorbing the lase beam energy or changing the light direction. Depending on the optical wavelength λ, the total attenuation coefficient can be shown as

$$\delta(\lambda) = \alpha_a + \alpha_b + \beta_a + \beta_b, \tag{2}$$

where α_a and α_b are the molecular and aerosol absorption coefficients, respectively. β_a and β_b, respectively denote the Rayleigh and Mie scattering coefficients. To describe the propagation loss, the Beer- Lambert law is applied as a function of the link length and attenuation coefficient, and can be shown as

$$h_a = \exp\left[\delta(\lambda) d_{fso}\right], \tag{3}$$

where d_{fso} is the distance from the transmitter, i.e., OGS, to the RIS-mounted building wall or from the RIS to the destination, i.e., UAVs (it is depending on the considered hop). The gas is similarly computed by considering the weather condition and propagation distance, d_{RD}, for the second hop from RIS to UAV. In our analysis, we chose the wavelength of 1550 nm to minimize the absorption and to satisfy the eye-safety requirement. Several typical values of the total attenuation coefficient in different weather conditions can be referred to in Table I [26].

Table 1. Typical values of the attenuation coefficient.

Weather conditions	$\delta(\lambda)$ (dB/km)
Heavy fog	125
Light fog	20
Heavy rain	9.2
Moderate rain	5.8
Haze	4.2
Clear air	0.43

C. Atmospheric turbulence

Inhomogeneity in the temperature and the pressure, the atmospheric turbulence causes random power fluctuation of the received signal. This leads to the redistribution of the signal energy. To fully describe the characteristic of turbulence-induced fading, gamma-gamma distribution is used in our analysis because of modeling a wide range of turbulence strength from weak to strong. The probability density function (PDF) of h_t can be expressed as

$$f_{h_t}(h_t) = \frac{2(\alpha\beta)^{\frac{\alpha+\beta}{2}}}{\Gamma(\alpha)\Gamma(\beta)} h_t^{\frac{\alpha+\beta}{2}} K_{\alpha-\beta}\left(2\sqrt{\alpha\beta h_t}\right), \tag{4}$$

where $K_{\alpha-\beta}(.)$ is the modified Bessel function of the second kind and order $(\alpha-\beta)$ and $\Gamma(.)$ is the gamma function. α and β represent effective number of large- and smallscale turbulence cell, and can be determined as

$$\alpha = \left\{\exp\left[\frac{0.49\sigma_R^2}{\left(1+1.11\sigma_R^{12/5}\right)^{7/6}}\right] - 1\right\}^{-1}, \tag{5}$$

$$\beta = \left\{\exp\left[\frac{0.51\sigma_R^2}{\left(1+0.69\sigma_R^{12/5}\right)^{5/6}}\right] - 1\right\}^{-1}, \tag{6}$$

where σ_R^2 is Rytov variance. For the plane wave, the Rytov variance can be determined as

$$\sigma_R^2 = 1.23\left(\frac{2\pi}{\lambda}\right)^{7/6} C_n^2 d_{fso}^{11/6}, \tag{7}$$

where C_n^2 is the index of refraction structure parameter.

D. Pointing Error Model

The first hop's pointing error due to the building sway vibration leads to RIS vibration. The misalignment between surface of RIS and the Gaussian beam center can be modeled by zero boresight pointing error as follow

$$f_{h_p}(h_p) = \frac{\xi^2}{A_0^{\xi^2}} (h_p)^{\xi^2 - 1}, 0 \le h_p \le A_0, \tag{8}$$

where A_0 is the fraction of the collected power. $\xi = \frac{w_{heq}}{2\sigma_R}$, σ_{ris} is the approximated RIS jitter variance. $v = \frac{a_{RIS}\sqrt{\pi}}{w_h\sqrt{2}}$, $w_{heq} = w_h\sqrt{\frac{\sqrt{\pi}erf(v)}{2v\exp(-v^2)}}$, $w_h = w_0\sqrt{1+\varepsilon\left(\frac{\lambda L_h}{\pi w_0^2}\right)^2}$, w_0 is the beam-waist at $L_h = 0$, λ is the optical wavelength, a_{RIS} is the radius of RIS surface, and ε is the coherence length [22].

The pointing error model can not use the same model due to UAV hovering. The misalignment between the center of reflected beam footprint and that of UAV detector leads to the pointing errors and considerably degrades the system performance. In our model, the misalignments illustrated in figure above are due to (i) the operation of UAV within a wide reflected beam coverage at a distance of ρ, which is not necessarily at the center of beam footprint, (ii) the hovering of UAV around a certain possition of UAV indicated by the displace ment vector $r_U = \left(r_{U_x}, r_{U_y}\right)$, in which r_{U_x} and r_{U_y} are modeled as independent zero-mean Gaussian random variable, i.e., $r_{U_x} \sim N\left(0, \sigma_{g_x}^2\right)$ and $r_{U_y} \sim N\left(0, \sigma_{g_y}^2\right)$, then the radial vector from this instantaneous position of UAV to the center of beam at **P** (in case of no vibration) can be expressed as $r_g = \left(r_{g_x}, r_{g_y}\right)$ with $r_{g_x} \sim N\left(\rho_x, \sigma_{g_x}^2\right)$ and $r_{g_y} \sim N\left(\rho_y, \sigma_{g_y}^2\right)$, and (iii) the vibration of reflected beam footprint modeled by the radial vector $r_{RIS} = \left(r_{R_x}, r_{R_y}\right)$ from its initial position at **P**, where $r_{R_x} \sim N\left(0, \sigma_{R_x}^2\right)$ and $r_{R_y} \sim N\left(0, \sigma_{R_y}^2\right)$ and the values of σ_{R_x} and σ_{R_y} can be expressed via the incident angle θ_{inc}. Thus, the total radial displacement vector is expressed as $r = r_g + r_{RIS}$ and its absolute value is shown as

$$\|r\| = \sqrt{\|r_g + r_{RIS}\|^2} = \sqrt{r_g^2 + 2\begin{bmatrix} r_{R_x} \\ r_{R_y} \end{bmatrix}^T \begin{bmatrix} r_{g_x} \\ r_{g_y} \end{bmatrix}^T + r_{RIS}^2} = \sqrt{\left(r_{g_x} + r_{R_x}\right)^2 + \left(r_{g_y} + r_{R_y}\right)^2}, \quad (9)$$

where $\|.\|$ is the norm of a vector, $[.]^T$ is the transpose of a matrix, $r_x = r_{g_x} + r_{R_x} \sim N\left(\rho_x, \sigma_{g_x}^2 + \sigma_{R_x}^2\right)$ and $r_y = r_{g_y} + r_{R_y} \sim N\left(\rho_y, \sigma_{g_y}^2 + \sigma_{R_y}^2\right)$. In our case, the

$$f_\gamma(\gamma) = \frac{1}{t\gamma_0^{1/t}\gamma^{1-1/t}} f_R\left[\left(\frac{\gamma}{\gamma_0}\right)^{1/t}\right] = \frac{\alpha_h\beta_h\alpha_g\beta_g\xi^2\varphi_m^2}{A_h h_a A_m g_a \Gamma(\alpha_g)\Gamma(\beta_g)\Gamma(\alpha_h)\Gamma(\beta_h)t\gamma_0^{1/t}}\gamma^{\frac{1}{t}-1} G_{2,6}^{6,0}\left[\frac{\alpha_h\beta_h\alpha_g\beta_g}{A_h h_a A_m g_a}\left(\frac{\gamma}{\gamma_0}\right)^{1/t}\middle| \begin{matrix} \xi^2, \varphi_m^2 \\ \xi^2-1, \alpha_h-1, \beta_h-1, \varphi_m^2-1, \alpha_g-1, \beta_g-1 \end{matrix}\right] \quad (15)$$

$$F_\gamma(\gamma_{th}) = \frac{\alpha_h\beta_h\alpha_g\beta_g\xi^2\varphi_m^2}{A_h h_a A_m g_a \Gamma(\alpha_g)\Gamma(\beta_g)\Gamma(\alpha_h)\Gamma(\beta_h)t\gamma_0^{1/t}}\gamma_{th}^{\frac{1}{t}} \times G_{3,7}^{6,1}\left[\frac{\alpha_h\beta_h\alpha_g\beta_g}{A_h h_a A_m g_a}\left(\frac{\gamma_{th}}{\gamma_0}\right)^{1/t}\middle| \begin{matrix} 1-1/t & \xi^2 & \varphi_m^2 \\ \xi^2-1 & \alpha_h-1 & \alpha_h-1 & \varphi_m^2-1 & \alpha_g-1 & \beta_g-1 & -1/t \end{matrix}\right] \quad (16)$$

horizontal and vertical displacement of r, i.e., r_x and r_y are two independent Gaussian random variables with different non-zero mean $\{\rho_x, \rho_y\}$ and variances $\{\sigma_x^2, \sigma_y^2\}$, where $\sigma_x^2 = \sigma_{g_x}^2 + \sigma_{R_x}^2$ and $\sigma_y^2 = \sigma_{g_y}^2 + \sigma_{R_y}^2$, then, r follow Beckmann distribution with PDF given as [23, 24]

$$f_r(r) = \frac{r}{2\pi\sigma_x\sigma_y} \times \int_0^{2\pi} \exp\left(-\frac{(r\cos\phi - \rho_x)^2}{2\sigma_x^2} - \frac{(r\sin\phi - \rho_y)^2}{2\sigma_y^2}\right) d\phi \quad (10)$$

The Beckman distribution can be accurately approximated by a modified Rayleigh distribution as follow

$$f_r(r) \approx \frac{r}{\sigma_m^2}\exp\left(-\frac{r^2}{2\sigma_m^2}\right), r \geq 0, \quad (11)$$

where $A_g = \left[erf(v_g)\right]^2$ is the fraction of the collected power at $r = 0$, $erf(x) = \frac{2}{\sqrt{\pi}}\int_0^x \exp(-t^2)dt$ is the error function, $w_{geq}^2 = w_g^2\frac{\sqrt{\pi}erf(v_g)}{2v_g\exp(-v_g^2)\cos^2(\theta_{rl})}$ is the equivalent beam-width [23] with the reflected angle, denoted as θ_{rl}. $v_g = \frac{a_U\sqrt{\pi}}{w_g\sqrt{2}}$ and w_g is the effective beam-width at the distance L_g, given as $w_g = w_0\sqrt{\left(\Theta_0^2 + \Lambda_0^2\right)\left(1 + 1.625\sigma_R^{12/5}\Lambda_1\right)}$ where σ_R^2 is the

Rytov variance, $w_0 = \frac{2\lambda}{\pi\theta_{divergence}}$ is the beam waist at $L_g = 0$ with $\theta_{divergence} = \theta_{source}\left(1+\frac{L_h}{L_g}\right)$ is the reflected divergence angle, $\Theta_0 = 1-\frac{L_g}{F_0}$ with F_0 is the raidus of curvature, $\Lambda_0 = \frac{2L_g}{k_{wave}w_0^2}$ with k_{wave} is the optical wave number, and $\Lambda_1 = \frac{\Lambda_0}{\Theta_0^2+\Lambda_0^2}$. From (8) and (9), the PDF of h_i^p can be derived as

$$f_{g_p}(g_p) = \frac{\varphi_m^2}{g_p}\left(\frac{g_p}{A_m}\right)^{\varphi_m^2}, \quad (12)$$

where $A_m = A_g \exp\left(\frac{1}{\varphi_m^2}-\frac{1}{2\varphi_x^2}-\frac{1}{2\varphi_y^2}-\frac{\rho_x^2}{2\sigma_x^2\varphi_x^2}-\frac{\rho_y^2}{2\sigma_y^2\varphi_y^2}\right)$, $\varphi_m = \frac{w_{geq}}{2\sigma_m}$, while $\varphi_x = \frac{w_{geq}}{2\sigma_x}$ and $\varphi_y = \frac{w_{geq}}{2\sigma_y}$ are the jitter variances in the x and y directions, respectively [26].

III. SYSTEM PERFORMANCE ANALYSIS

A. Composite Channel Model

The composite channel of the first hop from source to RIS can be similarly approached in [24] and can be expressed as,

$$f_h(h) = \frac{\alpha\beta\xi^2}{A_h h_a \Gamma(\alpha)\Gamma(\beta)} \times G_{1,3}^{3,0}\left[\frac{\alpha\beta}{A_h h_a}h_i\middle|\begin{matrix}\xi^2\\ \xi^2-1 & \alpha-1 & \beta-1\end{matrix}\right], \quad (13)$$

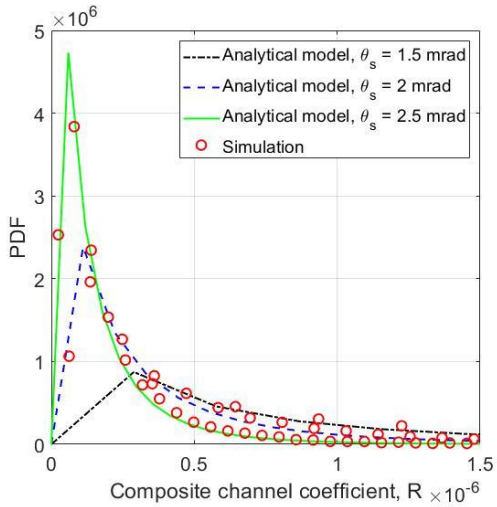

Figure 3. Confimation between analytical model and Monte-Carlo simulation.

Regarding the second hop from RIS to the destination, By applying [Eq. (9.31.5), 27] and [Eq. (21), 28], the composite PDF of $g = g_a g_t g_p$ can be shown as

$$f_g(g) = \frac{\alpha_h\beta_h\alpha_g\beta_g\xi^2\varphi_m^2}{A_h h_a A_m g_a \Gamma(\alpha_g)\Gamma(\beta_g)\Gamma(\alpha_h)\Gamma(\beta_h)} \times G_{2,6}^{6,0}\left[\frac{\alpha_h\beta_h\alpha_g\beta_g}{A_h h_i^a A_m g_i^a}g\middle|\begin{matrix}\xi^2,\varphi_m^2\\ \xi^2-1,\alpha_h-1,\beta_h-1,\varphi_m^2-1,\alpha_g-1,\beta_g-1\end{matrix}\right] \quad (14)$$

The figure 3 shows the accuracy of the analytical model comparision with monte-carlo (MC) simulation in different ground station's divergence angles. From these results, the analytical model completely matches with the MC model. From now on, we use the analytical model to plot the result.

B. Outage Probability

First, we derive the generalized formulation of PDF and CDF of the instantaneous SNR for two case of receiver's detection including (1) coherent heterodyne detection (HD) and (2) intensity modulation/direct detection (IM/DD). The PDF and CDF of the instantaneous can be expressed as in Eq. (15) and Eq. (16), where $t=1$ account for HD, and $t=2$ represents IM/DD.

The instantaneous SNR is defined as $\gamma = \gamma_0 R^t$ and $\gamma_0 = \frac{P^t}{N_0}$ denotes the average SNR. The outage probability can be expressed as

$$P_{out} = \Pr(\gamma < \gamma_{th}) = F_\gamma(\gamma_{th}), \quad (17)$$

IV. RESULTS AND DISCUSSIONS

The system parameters are setting as shown in Table 2 and other parameters are noted in each result.

Table 2. System Parameters.

Name	Symbol	Value
Bolzmann's constant	k_B	1.38×10^{-23} $WHz^{-1}K^{-1}$
Electronic charge	q	1.6×10^{-19} C
Light velocity	c	3×10^8 m/s
Load resistance	R_L	50 Ohm
Temperature	T	300 K
PD responsivity	$\Re$	0.8 A/W
Optical wavelength	λ	1550 nm
Transmission distance	d_{total}	3000 m
Aperture radius	A	10 cm
Background power	P_b	-30 dBm
SNR threshold	γ_{th}	0 dB

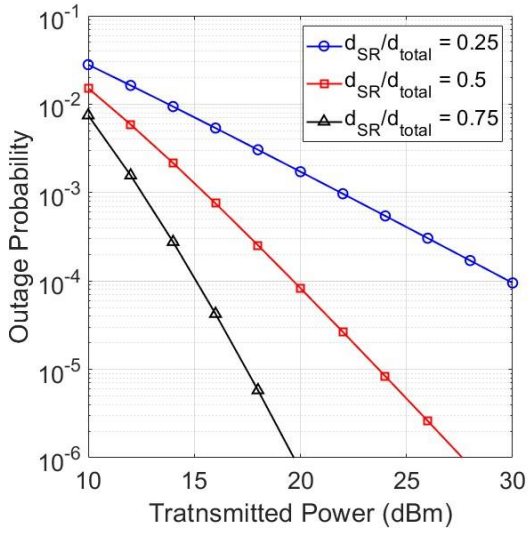

Figure 4. Outage probability versus transmitted power in the case of different position of RIS.

Figure 4 illustrates the outage performance in the case of the different positions of RIS over the range of the transmitted power from 10 to 30 dBm. In the figure, d_{SR} describe the distance from source to RIS, and d_{total} illustrate the propagation length from RIS to UAV. The RIS location decides the value of the virtual divergence angle, which emerges after the optical beam heads to the RIS surface. This led to the distance ratio between the source to RIS and RIS to the destination, an important parameter that needs to be investigated to see how the considered system's outage probability is going. Obviously, the outage performance reduces when the transmitted power increases. An interesting point from the result shows that the system's performance is better if RIS is located far from the source or RIS is situated near the destination. This can be explained by using Eq. (9); if the RIS is located near the destination, the virtual divergence angle is approximated by the source's divergence angle (i.e., it is small), the power is focused on the UAV lead to the good outage performance. For example, from this result, we can easily observe that the outage probability can achieve 10^{-3} with the transmitted power of 12.5 dBm, 15.5 dBm, and 22 dBm, corresponding to the ratio of d_{SR}/d_{total} of 0.25, 0.5, and 0.75.

The impact of weather conditions, i.e., fog condition, on the outage performance in the presence of the moderate and strong turbulence environment is shown in Fig. 5. Obviously, the outage probability is increased when the attenuation coefficient, denoted δ, grow up. It is can be proved via Eq. (3). Besides, the outage probability is seriously affected by turbulence-induced fading condition. As it predicted, the outage performance is quickly decreased when the turbulence strength down from strong regime $\left(C_n^2 = 10^{-14}\right)$ to moderate regime $\left(C_n^2 = 10^{-13}\right)$. The impact of fog condition on the outage performance will be stronger in the case of moderate turbulence than the strong turbulence regime.

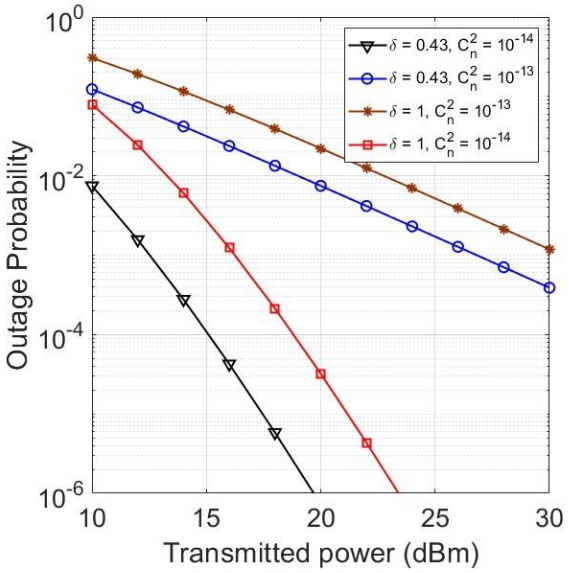

Figure 5. The impact of weather conditions, i.e., fog condition on the outage probability in the presence of moderate and strong turbulence environment.

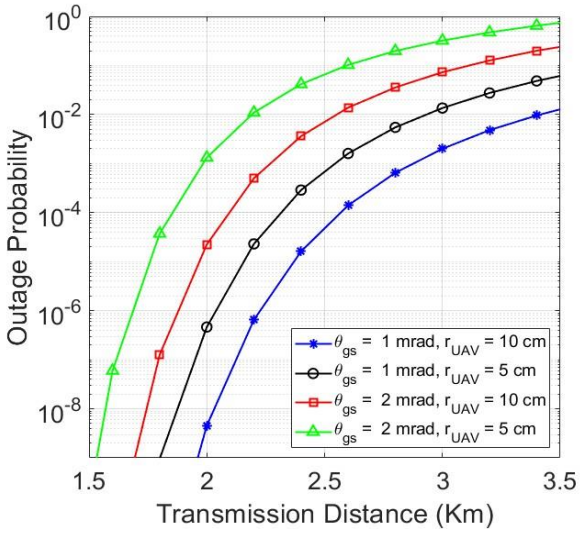

Figure 6. The relationship between outage probability and transmission distance in difference of divergence angle and UAV's aperture radius.

The relationship between outage probability and the total transmission distance is depicted in Fig. 6. In this result, we consider two cases of the different source's divergence angle with 1 mrad and 2 mrad and two values of UAV's receiver aperture radius of 5 cm and 10 cm. Basically, the transmission propagation length is longer; the outage performance is poor. Through the comparison between two cases of the source's divergence angle, we can see that the bigger the angle, the worse the system performance is. The reason behind this is that the bigger angle leads to more spreading out of the beam footprint; then, the UAV receives smaller power; however, we can serve more users in this case. If we use the smaller angle, the limited users are served; nevertheless, the outage

performance is ensured to reach the target because the focused power is collected at the UAV's detector. In addition, we investigate the different values of the UAV's aperture radius to express the impact of radius size on the outage performance. In fact, the bigger the radius, the better the outage performance is better due to the more power received at the destination. For instance, given the target outage probability of 10^{-6} and the ground station's divergence angle of 1 mrad, the maximum transmission distance can reach 2.05 Km and 2.25 Km, respective to the design of UAV's radius size of 5 cm and 10 cm.

V. CONCLUSION

In this work, we have examined the performance of the RIS-assisted FSO-based integrated vehicular network in terms of outage probability under the influence of propagation loss, atmospheric turbulence, RIS vibration, and UAV hovering. The medium contains a wide variety of impediments and particles, which hinder or obstruct the optical signal. By adding RIS elements, a RIS-based approach exacerbates the system performance. The outage probability characteristics of RIS-based FSO links have been computed and plotted with respect to transmitted power and transmission distance. We have displayed the outage probability performances for various system parameters such as divergence angle, UAV's aperture radius, distance ratio, etc., to investigation the system performance comprehensively. In the face of many impacts, the suggested RIS-assisted FSO-based ground-air integrated vehicular networks guarantee improved information integrity for urban areas.

For the future works, it is interesting to explore more impact of the environment conditions as well as the hardware impairment on the considered system. In addition, several system's performance metrics can be calculated such as bit error rate (BER), capacity, and so on.

REFERENCES

[1] X. Zhang, L. Han, H. Wei, X. Tan, W. Zhou, W. Li, and Y. Qian, "Linking urbanization and air quality together: a review and a perspective on the future sustainable urban development," J. Cleaner Prod. 346, 130988 (2022).

[2] S. T. Pickett and W. Zhou, "Global urbanization as a shifting con- text for applying ecological science toward the sustainable city," Ecosystem Health Sustain. 1, 1–15 (2015).

[3] A. Kumar and P. Krishnan, "Performance analysis of RoFSO links with spatial diversity over combined channel model for 5G in urban area applications," Opt. Commun. 466, 125600 (2020).

[4] H. Wang, Z. Zhang, B. Zhu, J. Dang, L. Wu, L. Wang, K. Zhang, and Y. Zhang, "Performance of wireless optical communication with recon- figurable intelligent surfaces and random obstacles," arXiv preprint arXiv:2001.05715 (2020).

[5] M. R. Bhatnagar and Z. Ghassemlooy, "Performance analysis of gamma–gamma fading FSO MIMO links with pointing errors," J. Lightwave Technol. 34, 2158–2169 (2016).

[6] Q. Wu, S. Zhang, B. Zheng, C. You, and R. Zhang, "Intelligent reflect- ing surface-aided wireless communications: a tutorial," IEEE Trans. Commun. 69, 3313–3351 (2021).

[7] E. Basar, M. Di Renzo, J. De Rosny, M. Debbah, M.-S. Alouini, and R. Zhang, "Wireless communications through reconfigurable intelligent surfaces," IEEE Access 7, 116753 (2019).

[8] Y.-C. Liang, R. Long, Q. Zhang, J. Chen, H. V. Cheng, and H. Guo, "Large intelligent surface/antennas (LISA): making reflective radios smart," J. Commun. Inf. Netw. 4, 40–50 (2019).

[9] M. Najafi, B. Schmauss, and R. Schober, "Intelligent reflecting sur- faces for free space optical communication systems," IEEE Trans. Commun. 69, 6134–6151 (2021).

[10] Tuan-Lam Vu, Trung-Anh Do, Thang. V. Nguyen, Tien-Sy Dang, and Ngoc T. Dang, "Outage Performance of IRS-Assisted Underwater Optical Wireless Communication Systems over Combined Channel Model," In the Proc. of the IEEE 19th International Conference on Wireless and Mobile Computing, Networking and Communications (WiMob), Montreal, Canada, June 2023, pp. 318-323..

[11] L. P. Kumar, R. P. Naik, P. Krishnan, A. B. Raj, A. K. Majumdar, and W. Y. Chung, "RIS assisted triple-hop RF-FSO convergent with UWOC system," IEEE Access 10, 66564–66575 (2022).

[12] Z. Cao, X. Zhang, G. Osnabrugge, J. Li, I. M. Vellekoop, and A. M. Koonen, "Reconfigurable beam system for non-line-of-sight free-space optical communication," Light Sci. Appl. 8, 69 (2019).

[13] M. Di Renzo, A. Zappone, M. Debbah, M.-S. Alouini, C. Yuen, J. De Rosny, and S. Tretyakov, "Smart radio environments empowered by reconfigurable intelligent surfaces: how it works, state of research, and the road ahead," IEEE J. Sel. Areas Commun. 38, 2450–2525 (2020).

[14] B. Di, H. Zhang, L. Song, Y. Li, Z. Han, and H. V. Poor, "Hybrid beamforming for reconfigurable intelligent surface based multi- user communications: achievable rates with limited discrete phase shifts," IEEE J. Sel. Areas Commun. 38, 1809–1822 (2020).

[15] H. Zhang, B. Di, Z. Han, H. V. Poor, and L. Song, "Reconfigurable intelligent surface assisted multi-user communications: how many reflective elements do we need?" IEEE Wireless Commun. Lett. 10, 1098–1102 (2021).

[16] H. Zhang, B. Di, L. Song, and Z. Han, "Reconfigurable intelligent sur- faces assisted communications with limited phase shifts: how many phase shifts are enough?" IEEE Trans. Veh. Technol. 69, 4498–4502 (2020).

[17] K. O. Odeyemi, G. Aiyetoro, P. A. Owolawi, and O. O. Olakanmi, "Performance analysis of reconfigurable intelligent surface in a dual-hop DF relay empowered asymmetric RF/FSO networks," Opt. Quantum Electron. 53, 1–17 (2021).

[18] C. Stefanovic, M. Morales-Céspedes, and A. G. Armada, "Performance analysis of RIS-assisted FSO communications over Fisher–Snedecor F turbulence channels," Appl. Sci. 11, 10149 (2021).

[19] A. Al-Habash, L. C. Andrews, and R. L. Phillips, "Mathematical model for the irradiance probability density function of a laser beam propa- gating through turbulent media," Opt. Eng. 40, 1554–1562 (2001).

[20] K. Prabu, D. S. Kumar, and T. Srinivas, "Performance analysis of FSO links under strong atmospheric turbulence conditions using various modulation schemes," Optik 125, 5573–5581 (2014).

[21] W. O. Popoola and Z. Ghassemlooy, "BPSK subcarrier intensity modulated free-space optical communications in atmospheric turbulence," J. Lightwave Technol. 27, 967–973 (2009).

[22] L.Han,X.Liu,Y.Wang,andX.Hao,"Analysisofris-assistedfsosystems over f turbulence channel with pointing errors and imperfect csi," IEEE Wireless Communications Letters, pp. 1–1, 2022.

[23] I.S.Ansari,F.Yilmaz,andM.-S.Alouini,"Performanceanalysisoffree- space optical links

over ma´laga (M) turbulence channels with pointing errors," IEEE Transactions on Wireless Communications, vol. 15, no. 1, pp. 91–102, 2016.
[24] T. V. Nguyen, T. V. Pham, N. T. Dang, and A. T. Pham, "Performance of generalized qam/fso systems with pointing misalignment and phase error over atmospheric turbulence channels," IEEE Access, vol. 8, pp. 203631– 203644, 2020.
[25] A. Mansour, R. Mesleh, and M. Abaza, "New challenges in wireless and free space optical communications," Optics and Lasers in Engineering, vol. 89, pp. 95 – 108, 2017.
[26] Ruben B. Ruiz et. al., "Novel approximation of misalignment fading modeled by Beckmann distribution on free-space optical links," Optics Express.
[27] I. S. Gradshteyn, et. al., *Table of integrals series and productions*, Academic press, 2007.
[28] Adamchik V. S., et. al., "The algorithm for calculating integrals of hypergeometric type functions and its realization in reduce system" 1990.

PHÂN TÍCH HIỆU SUẤT CỦA MẠNG PHƯƠNG TIỆN TÍCH HỢP MẶT ĐẤT-TRÊN KHÔNG DỰA TRÊN RIS-HỖ TRỢ FSO

Tóm tắt-. Những trở ngại đáng kể đối với thiết kế thực tế của thông tin quang trong không gian tự do (FSO) bao gồm nhiễu loạn khí quyển và các vấn đề về lỗi lệch hướng. Bề mặt thông minh có thể cấu hình lại (RIS) là một công nghệ mới nổi sử dụng vật liệu phản xạ thụ động rẻ tiền để thay đổi hướng chùm tia một cách thông minh theo hướng thích hợp, tạo điều kiện truyền sóng vô tuyến phản xạ cho hệ thống không dây 5G/6G thế hệ tiếp theo. Trong nghiên cứu này, chúng tôi đã đề xuất một hệ thống FSO có hỗ trợ RIS để giảm thiểu tác động của việc nghẽn tín hiệu trong hệ thống liên lạc, nhiễu loạn không khí và lỗi chỉ đường. Trong môi trường không gian tự do có chướng ngại vật, hàm mật độ xác suất và hàm phân bố tích lũy của hệ thống FSO được tạo thành từ các phần tử RIS được đánh giá. Chúng tôi đã thu được các công thức dạng tường minh của xác suất ngừng hoạt động của hệ thống được đề xuất. Việc phân tích hiệu năng của hệ thống được đề xuất trong các điều kiện thời tiết khác nhau, lỗi định hướng và tắc nghẽn tín hiệu được thực hiện dưới dạng BER, xác suất ngừng hoạt động và dung lượng kênh. Các phát hiện được trình bày liên quan đến tỷ lệ tín hiệu trên tạp âm trung bình và số lượng phần tử RIS. Bởi vì hệ thống được đề xuất sẽ cung cấp khả năng kết nối đáng tin cậy trong môi trường đô thị với dân số đông đúc và các công trình kiến trúc cao tầng, nên nó sẽ thuận lợi cho các ứng dụng ở các khu vực đông dân cư.

Từ khóa- Bề mặt phản xạ thông minh (RIS), truyền thông quang vô tuyến (FSO), mạng phương tiện.

Nguyen Van Thang received B.E. from Posts and Telecommunications Institute of Technology (PTIT), Vietnam, in 2017. He obtained M.E. and Ph.D. degrees in Computer Science and Engineering from the University of Aizu (Japan) in 2019 and 2022, respectively. Now, he is a lecturer at PTIT and researcher at wireless system and applications laboratory. His current research interests include the aera of communication theory with a particular emphasis on modeling, design and performance analysis of hybrid FSO/RF systems, optical wireless communications, satellite communications.

Pham Thi Thuy Hien received the B.E. Degree from Hanoi University of Transport and Communications in 1999; and the M.E. and Ph.D. degrees in Telecommunication Engineering from Posts and Telecommunications Institute of Technology (PTIT) in 2005 and 2017, respectively. She has been working at the Department of Wireless Communications of PTIT since 1999. Dr. Pham is currently a senior lecturer at PTIT. Her present research interests are in the area of design and performance evaluation of optical and wireless communication systems.